A BACKWARDS APPROACH TO THE FORMATION OF DISK GALAXIES I. STELLAR AND GAS CONTENT

IGNACIO FERRERAS & JOSEPH SILK
Nuclear & Astrophysics Lab. Keble Road, Oxford OX1 3RH, England, UK

(Accepted for publication in the Astrophysical Journal)

ABSTRACT

A simple chemical enrichment code is described where the two basic mechanisms driving the evolution of the ages and metallicities of the stellar populations are the star formation efficiency and the fraction of gas ejected from the galaxy. Using the observed Tully-Fisher relation in different passbands as a constraint, it is found that a steep correlation between the maximum disk rotational velocity ($v_{\rm ROT}$) and star formation efficiency ($C_{\rm eff}$) must exist — $C_{\rm eff} \propto v_{\rm ROT}^4$ — either for a linear or a quadratic Schmidt law. Outflows do not play a major role. This result is in contrast with what we have found for early-type systems, where the Faber-Jackson constraint in different bands allows a significant range of outflows and requires a large star formation efficiency regardless of galaxy mass. The extremely low efficiencies found at low masses translate into a large spread in the distribution of stellar ages in these systems, as well as a large gas mass fraction independently of the star formation law. The model predictions are consistent with the star formation rates in low-mass local galaxies. However, our predictions for gas mass are in apparent conflict with the estimates of atomic hydrogen content observed through the flux of the 21cm line of H I. The presence of large masses of cold molecular hydrogen — especially in systems with low mass and metallicity — is predicted, up to ratios M(H_2)/M(HI)~ 4, in agreement with a recent tentative detection of warm H_2. The redshift evolution of disk galaxies is explored, showing that a significant change in the *slope* of the Tully-Fisher relation ($L \propto v_{\rm ROT}^{\gamma}$) is expected because of the different age distributions of the stellar components in high and low-mass disk galaxies. The slope measured in the rest frame B,K-bands is found to change from $\gamma_B \sim 3, \gamma_K \sim 4$ at $z = 0$ up to $\sim 4.5, 5$ at $z \sim 1$, with a slight dependence on formation redshift.

Subject headings: galaxies: evolution — galaxies: formation — galaxies: spiral — galaxies: stellar content — galaxies: fundamental parameters.

1. INTRODUCTION

The process of galaxy formation can be divided into two distinct and equally important histories. On the one hand, the dynamical history of galaxies is crucial in understanding the Hubble sequence (or other morphological classifications) that we see now as well as its evolution with redshift. On the other hand, the star formation history allows us to trace the baryonic matter, its conversion from gas to stars and the feedback from stellar evolution in the processing of subsequent generations of stars. Disk galaxies are assumed to be the building blocks from which the rest of the galactic "zoo" we see around us has been assembled. The standard picture of disk galaxy formation involves the infall and cooling of primordial gas onto the centers of dark matter halos and its later conversion into stars (White & Rees 1978). A multitude of models have been published, describing this process in varying degrees of detail, following either a dynamical approach, where gravity plays the dominant role in the properties of galaxies, or a spectrophotometric approach, where the key issue is the highly complex and so far unsolved problem of star formation. The former approach usually over-simplifies the luminous properties of galaxies by assuming a fixed value of the mass-to-light ratio, tying the properties of the observed parts of galaxies to the behavior of the much larger halos in which the luminous matter is embedded. On the other hand, models based on the evolution of the stellar populations lack the dynamical information needed in order to quantify the merger tree. Semi-analytic models (e.g. Kauffmann et al. 1999; Baugh et al. 1998) attempt to fill in the gap between these two approaches at the expense of a large and complicated set of parameters.

We follow a spectrophotometric approach, defining a model that traces both the evolution of gas and metal content in a simple star formation scenario reduced to infall of primordial gas that fuels star formation via a simple power law dependence on gas content. The model allows for outflows of gas driven out of the galaxy, whose cause could either be stellar (feedback from supernova-driven winds) or dynamical (e.g. merging or harassment). In this paper we study the evolution of the gas and stellar content in disk galaxies, ignoring size evolution. In a future paper (Ferreras & Silk, in preparation) we use the same model to explore the evolution of sizes and surface brightnesses along with the associated effects on the selection function of current surveys at moderate and high redshift.

The first part of this paper (§§2,3,4) describes the model as well as the technique used in order to constrain the volume of parameter space sampled. In §5 we discuss the star formation efficiencies predicted by the model. §6 explores the issue of gas content in disk galaxies and speculates on the idea that a large fraction of gas could be found in the form of cold H_2. §7 explains the redshift evolution predicted by our model for the star formation rates as well as for the Tully-Fisher relation. Finally §8 is a brief summary of our results with a discussion of the most interesting issues, regarding disk galaxy formation, raised by our work.

2. MODELLING STAR FORMATION IN DISK GALAXIES

We follow a chemical enrichment code similar to the one described in more detail in Ferreras & Silk (2000a,b), where the formation and evolution of the stellar populations is parametrized by a range of star formation efficiencies ($C_{\rm eff}$) and outflows ($B_{\rm out}$). The model only traces the cold gas component

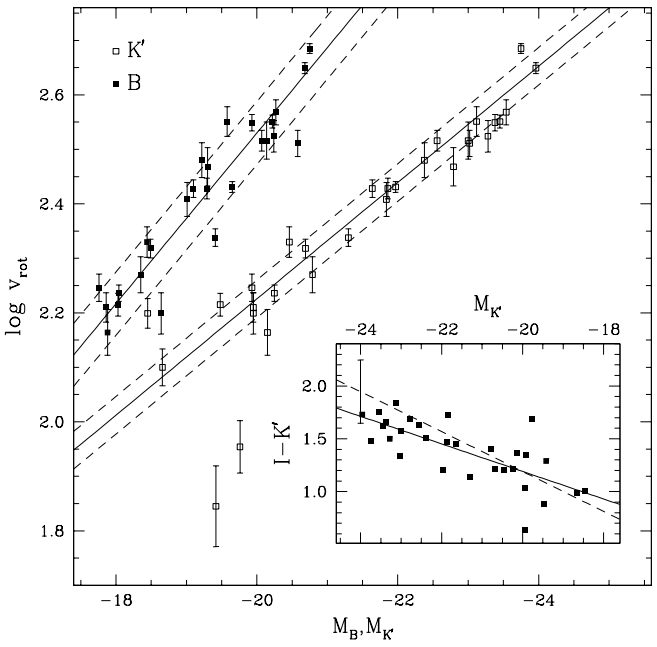

FIG. 1.— The Tully-Fisher relation in different broadbands from the sample of disk galaxies in the Ursa Major cluster (Verheijen 1997). For clarity purposes we have plotted only B and K' data, although the analysis presented here uses the full range of filters: $\{B,R,I,K'\}$. The solid and dashed lines represent the linear fits and scatter used as constraint. The inset shows the $I-K'$ color-magnitude relation inferred by comparing the Tully-Fisher relation in I and K' bands. The linear fit of the $I-K'$ vs $M_{K'}$ color-magnitude relation from the data (solid line) and from de Grijs & Peletier (1999; dashed line) using a completely different sample of disk galaxies is consistent within the scatter of the data, shown as an error bar.

that gives rise to star formation, with instantaneous mixing of the ejected gas from stars and the cold gas component being assumed. The gas mass density (μ_g) and metallicity (Z_g) obey a simple set of chemical enrichment equations following the formalism of Tinsley (1980):

$$\frac{d\mu_g}{dt} = -\psi(t) + (1-B_{\rm out})E(t) + f(t), \qquad (1)$$

where $\psi(t)$ is the star formation rate, $f(t)$ the gas infall rate, $E(t)$ the gas mass ejected from stars of all masses, and $B_{\rm out}$ is the fraction of gas ejected from the galaxy. Since this paper treats galaxies as unresolved objects, and we do not assume a threshold in density for the star formation rate, we can always interchange mass densities and total masses. The evolution of the metallicity follows a similar equation:

$$\frac{d(Z_g\mu_g)}{dt} = -Z_g(t)\psi(t) + Z_f f(t) + (1-B_{\rm out})E_Z(t), \qquad (2)$$

where Z_f is the metallicity of the infalling gas (assumed to be primordial in this paper), and $E_Z(t)$ is the mass in metals ejected from stars. Infall of primordial gas fuels star formation via a Schmidt-type law (Schmidt 1959):

$$\psi(t) = C_{\rm eff}\mu_g^n(t); \qquad (3)$$

where $C_{\rm eff}$ is the star formation efficiency parameter. We assume either a linear (n = 1) or a quadratic law (n = 2) as extreme examples. The power law index that best fits observational data (n = 1.4) lies between these two values (Kennicutt 1998a). In the instantaneous recycling approximation — for which the stellar lifetimes are assumed to be either zero or infinity, depending on whether the stellar mass is greater or less than some mass threshold (M_0) — the star formation rate can be solved analytically (e.g. Tinsley 1980). Taking n = 1:

$$\psi(t) = C_{\rm eff}\int_0^t ds\, f(t-s)\exp(-s/\tau_g), \qquad (4)$$

$$\tau_g^{-1} = C_{\rm eff}\left[1-(1-B_{\rm out})R\right]; \qquad (5)$$

where R is the returned mass fraction from stars with masses $M > M_0$. Hence, the inverse of $C_{\rm eff}$ is roughly the time (in Gyr) needed to process gas into stars. The comparison between the efficiency defined here ($C_{\rm eff}$) and observed efficiencies — such as the parameter A defined in Kennicutt (1998b) with respect to surface densities rather than total masses, i.e. $A = \Sigma_\psi/\Sigma_{\rm gas}^n$ — is straightforward without a star formation threshold, but gets rather complicated with such a threshold, which causes $C_{\rm eff}$ to lie systematically below the observed efficiencies by a factor given by the ratio between the surface of the disk with density above threshold with respect to the total area. If we assume a universal star formation law, one would expect a systematic offset between observed star formation efficiencies and model one-zone efficiencies such as our $C_{\rm eff}$.

The infall rate that fuels star formation is assumed to have a Gaussian profile peaked at an epoch described by a formation redshift parameter (z_F), with two different timescales for ages earlier or later than the time corresponding to that formation redshift, namely:

$$f(t) \propto \begin{cases} \exp[-(t-t(z_F))^2/2\tau_1^2] & t < t(z_F) \\ \exp[-(t-t(z_F))^2/2\tau_2^2] & t > t(z_F). \end{cases} \qquad (6)$$

For $t < t(z_F)$ we assume a short infall timescale — τ_1 = 0.5 Gyr — which results in a prompt enrichment of the interstellar medium and thereby circumvents the G dwarf problem. Any model of chemical enrichment must avoid the overproduction of low metallicity stars by assuming either a non-monotonically decreasing star formation rate (as in this paper) or initially non-primordial gas (pre-enrichment). For $t > t(z_F)$ the infall timescale (τ_2) is a rough label for disk type: early-type disks will be associated with short timescales ($\tau_2 \sim 1-2$ Gyr), whereas late-type disks, with more extended star formation histories, correspond to larger values of τ_2. The Initial Mass Function (IMF) used is a hybrid between a Salpeter (1955) and a Scalo (1986) IMF. The high-mass end follows a Salpeter power law, with upper-mass cutoff at $60M_\odot$, whereas the low-mass end — truncated at $0.1M_\odot$ — follows the Scalo IMF. Stellar lifetimes follow a broken power law fit to the data from Tinsley (1980) and Schaller et al. (1992). We refer the reader to Ferreras & Silk (2000a,b) for more details about the chemical enrichment code.

The outflow parameter ($B_{\rm out}$) is used to quantify the amount of gas ejected out of stars and that leaves the galaxy and does not contribute to the processing of the next generation of stars. This mechanism plays an important role in the mass-metallicity correlation as originally suggested by Larson (1974): massive galaxies are expected to retain most of the gas, thereby increasing the average metallicity, whereas the shallow gravitational wells of low-mass galaxies cannot prevent enriched gas from being ejected from the galaxy, resulting in lower average metallicities. It is a well-known fact that the color range found in early-type systems is mostly driven by metallicity

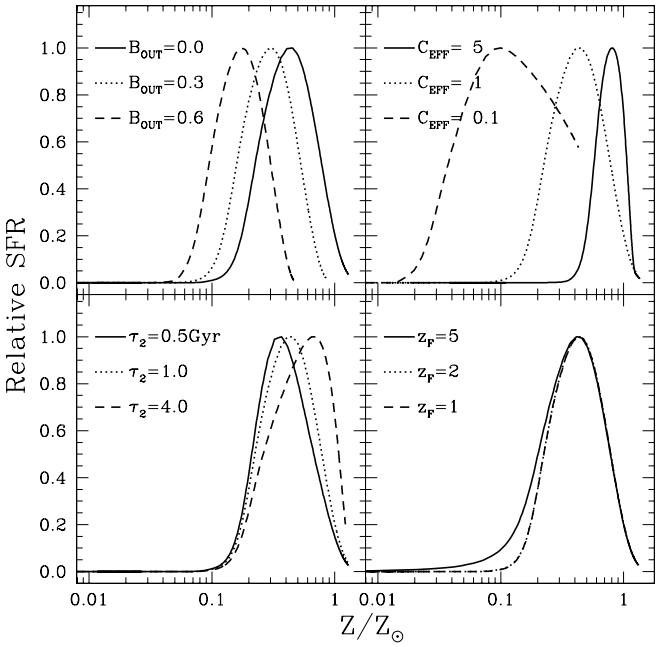

FIG. 2.— Histogram of metallicities of the stellar populations following the chemical enrichment code described here (using a linear Schmidt-type law) for a range of outflows ($B_{\rm out}$; *top left*); star formation efficiencies ($C_{\rm eff}$; *top right*); infall timescale (τ_2, *bottom left*); and epoch at peak of infall, given as a formation redshift (z_F). The fiducial set of parameters is ($B_{\rm out}$,$C_{\rm eff}$,τ_2,z_F)=(0,1,1 Gyr,2).

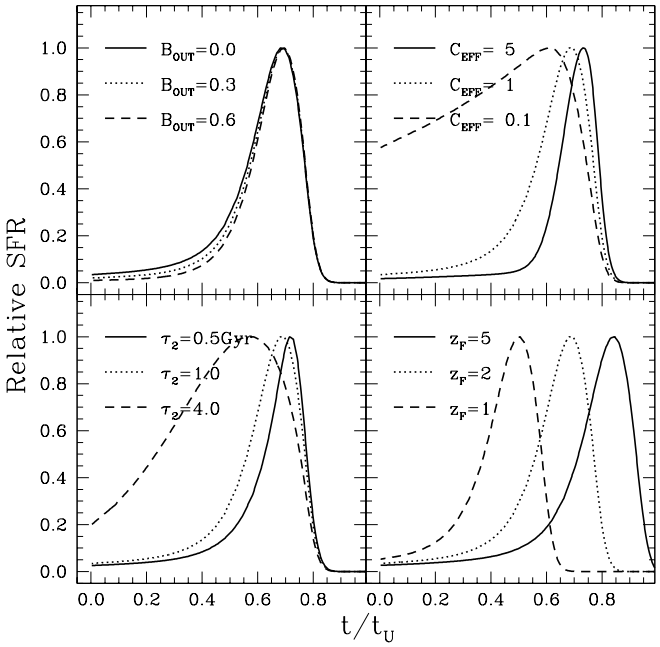

FIG. 3.— Age histogram of the stellar populations for the same range of parameters as in Figure 2. The ages are given with respect to the age of the universe at zero redshift: t_U, which is 13.5 Gyr for a H_0 = 70 km s^{-1}Mpc^{-1}; Ω_m = 0.3, Λ-dominated flat cosmology, used throughout the paper.

(e.g. Kodama et al. 1998), and can be explained by a correlation between the outflow parameter ($B_{\rm out}$) and the total mass of the system (Ferreras & Silk 2000b).

The chemical enrichment process in galaxies is hence described in this model with a set of five parameters: ($\tau_1, \tau_2, z_F, C_{\rm eff}, B_{\rm out}$). Only the early-infall timescale — τ_1 — is fixed to 0.5 Gyr throughout, whereas the other four parameters are allowed to vary over a large range of values. Every set of parameters chosen describes a star formation history ($\psi(t)$, $Z_g(t)$) which can be used to convolve simple stellar populations in order to find the composite spectral energy distribution of a galaxy whose formation process corresponds to that choice of parameters. We use the latest population synthesis models from Bruzual & Charlot (in preparation), which span the range of metallicities $\frac{1}{50} \leq Z/Z_\odot \leq \frac{5}{2}$ and include all phases of stellar evolution, from the zero-age main sequence to supernova explosions for progenitors more massive than $8M_\odot$, or to the end of the white dwarf cooling sequence for less massive progenitors. The uncertainties present in population synthesis models (Charlot, Worthey & Bressan 1996) complicate the determination of absolute values for parameters such as stellar ages or star formation efficiencies. This paper aims at showing *relative* values of efficiencies or outflow parameters between galaxies of different masses.

The predicted spectral energy distribution obtained for each point scanned in this large volume of parameter space is matched against observed data so that a map of the parameter range compatible with observations can be drawn. Here we use the Tully-Fisher relation of disk galaxies in different passbands as a constraint, shown in Figure 1. The data involve multiband $\{B,R,I,K'\}$ photometry of a sample of disk galaxies in the Ursa Major cluster (Verheijen 1997). Section 4 describes the comparison in more detail.

3. OUTFLOWS VERSUS STAR FORMATION EFFICIENCIES

In order to visualize the role of every parameter used in the chemical enrichment model presented here, we show in Figures 2 and 3 the metallicity and age distribution, respectively, for a range of outflows ($B_{\rm out}$); star formation efficiencies ($C_{\rm eff}$) and infall parameters (τ_2, z_F). The fiducial set chosen is ($B_{\rm out}$,$C_{\rm eff}$,τ_2,z_F)= (0,1,1 Gyr,2). In each panel, one of the parameters is allowed to vary, while keeping the others fixed. Notice the effect of the early-infall timescale (τ_1) on the metallicity distribution, which avoids the over-production of low metallicity stars. If we had set the timescale τ_1 to zero, the metallicity histogram would have been a monotonically decreasing function, peaked at zero metallicity. Closed-box models with constant star formation efficiencies and a standard initial mass function always yield monotonically decreasing star formation rates that over-produce low metallicity stars which contradict observations, both in our local stellar census (Rocha-Pinto & Maciel 1996) as well as in the integrated photometry of bulge-dominated galaxies (Worthey, Dorman & Jones 1996). Models with pre-enriched gas fuelling star formation generate similar distributions although shifted towards higher abundances. The photometric predictions of pre-enrichment models can be made compatible with the observations. However, the metallicity distribution — a monotonically decreasing function with Z with the maximum at the pre-enriched metallicity — is in disagreement with the observed metallicities of stars in the Milky Way (e.g. Rocha-Pinto & Maciel 1996). However, see Rich (1990) and Ibata & Gilmore (1995), who find an agreement between the prediction of a closed-box model and the distribution in the galactic bulge.

The top left panels of Figures 2 and 3 show that a range in outflows — with all the other parameters fixed — does not generate significantly different age distributions. The net effect of a change in the amount of gas ejected from the galaxy is a shift

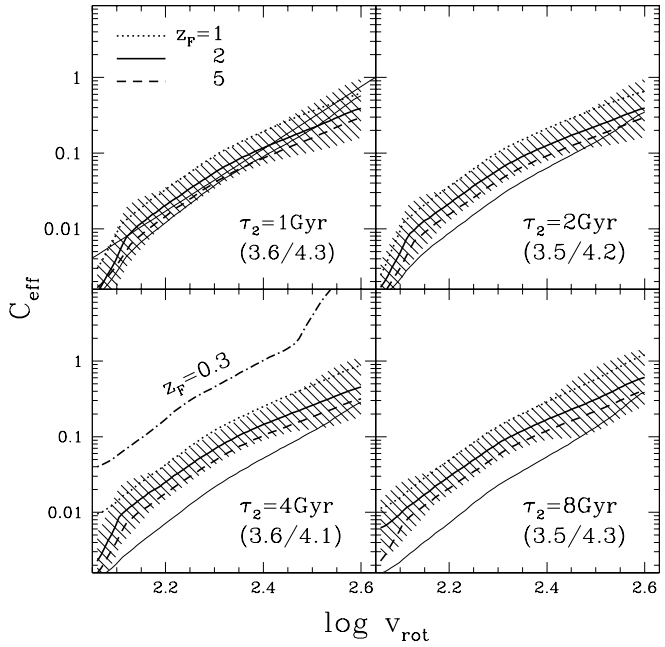

FIG. 4.— Range of star formation efficiencies ($C_{\rm eff}$) as a function of rotational velocity obtained using the multi-band Tully-Fisher relation as constraint with a linear Schmidt-type law. The thick dotted, solid and dashed lines correspond to formation redshifts of z_F = 1, 2 and 5, respectively. The shaded area represents the 90% confidence level in the χ^2 fit for z_F = 2. The thin solid line gives the range of efficiencies in the model with z_F = 2 using a quadratic Schmidt-type law. The numbers in parentheses for every infall timescale give the slope $\Delta \log C_{\rm eff}/\Delta \log v_{\rm ROT}$ for z_F = 2, using a linear and quadratic Schmidt law, respectively. The dot-dash line in the bottom-left panel shows how a very late formation redshift (z_F = 0.3) results in an increase of the star formation efficiency.

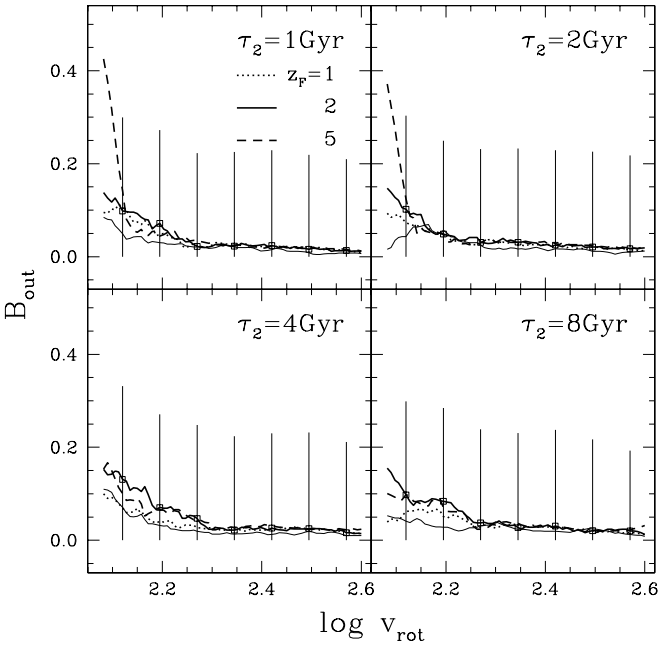

FIG. 5.— Range of outflows as a function of rotational velocity for four different infall timescales (linear Schmidt law). The error bars are the 90% confidence levels in the χ^2 analysis for the z_F = 2 case. The dotted, solid and dashed lines represent different formation redshifts (z_F = 1, 2 and 5, respectively). The thin solid line is the result for a quadratic Schmidt-type law with z_F = 2.

in the average metallicity. Hence, the assumption that an outflow range is the only mechanism driving the luminosity sequence of galaxies results in a pure metallicity sequence. On the other hand, a range of star formation efficiencies generates distributions with different ages and metallicities. The efficiency parameter sets the clock rate at which stars are being formed from the infalling gas (equations 4 and 5). Hence, systems with lower efficiencies generate a larger age spread, and lower average metallicities. Finally, the parameters controlling infall (τ_2 and z_F) simply shift the age distributions without a significant change in the metallicities, as expected, since $B_{\rm out}$ and $C_{\rm eff}$ are the only parameters driving the chemical enrichment process: it is possible to re-define the time variable as $s \equiv (t - t(z_F))/\tau_2$ and solve similar chemical enrichment equations to (1) and (2) with respect to variable s, without any significant dependence on the infall parameters (τ_2 and z_F).

A comparison of the age and metallicity histograms with the observed mass-metallicity correlation found in disk galaxies (Zaritsky, Kennicutt & Huchra 1994) suggests that either outflows and/or star formation efficiencies must be strongly correlated with galaxy mass. However, one can not determine *a priori* whether the observed color range found in disks is purely driven by outflows (i.e. a metallicity sequence) or by efficiency (i.e. a mixed age + metallicity sequence).

4. THE TULLY-FISHER RELATION AS A CONSTRAINT

The work described here follows a "backwards" approach in that we apply correlations between observables in local galaxies as a constraint and use the chemical enrichment code in order to evolve the system backwards in time. For disk galaxies the obvious constraint to be used is the Tully-Fisher relation (Tully & Fisher 1977): this shows a tight correlation between the disk rotation velocity — which is a measure of the ratio between the mass and the size of the galaxy — and the absolute luminosity. The scatter of this correlation is rather small (~ 0.3 mag) which allows it to be used as a distance indicator with uncertainties as low as 10%, notwithstanding unknown systematic effects (e.g. Jacoby et al. 1992). The small scatter hides a fundamental connection between the dynamical evolution of disk galaxies and their star formation histories. The analogous correlation for bulges or early-type systems — the Faber-Jackson relation (Faber & Jackson 1976) between luminosity and velocity dispersion of the spheroid — has a larger scatter, a clear sign of a more complex dynamical evolution.

The conventional scenario for disk formation via infall of gas onto the centers of dark matter halos gives a qualitative idea of the trend followed by the Tully-Fisher relation: massive disks (which have faster rotation velocities) will create more stars, thereby having higher luminosities than low-mass systems. However, a more detailed analysis of the Tully-Fisher relation — including disk sizes which of course affect the measured rotation velocity — shows that the interpretation of the slope and zero point of the Tully-Fisher relation is more complicated. Many dynamical models assume constant mass-to-light ratios (M/L), an incorrect assumption unless only stellar populations of the same ages dominate the light from all disks. The Tully-Fisher relation observed through near-infrared passbands minimizes the effect of the chemical enrichment history, and so K-band is the preferred filter in order to use the correlation as a distance indicator. Rather than exploring a suitable way of finding a "distilled" Tully-Fisher relation that is independent of the formation process, we will use the correlation in different

filters in order to constrain the star formation history of disk galaxies. There are many samples of disk galaxies for which rotation curves have been observed using different techniques such as optical emission lines (Mathewson & Ford 1996) or the 21 cm line of atomic hydrogen (Giovanelli et al. 1997). We use the sample of disk galaxies in the Ursa Major cluster (Tully et al. 1996; Verheijen 1997) imaged in several filters: *B*, *R*, *I* and K'. The rotation curves were determined with the 21 cm line of H I.

For a choice of parameters describing the star formation history: ($B_{\rm out}$, $C_{\rm eff}$, τ_2, z_F), we solve equations (1) and (2) describing the evolution of the gas mass and metallicity and use this to convolve simple stellar populations from the latest models of Bruzual & Charlot (in preparation). We explore four different formation redshifts ($z_F = \{1,2,3,5\}$) and four different infall timescales ($\tau_2 = \{1,2,4,8\}$ Gyr), corresponding to a range of galaxy types: from early-type disks such as S0, Sa — for $\tau_2 \sim 1-2$ Gyr — to late-type systems such as Sd for longer timescales. For every pair of values describing infall ($\{\tau_2, z_F\}$) we scan a grid of 128×128 star formation efficiencies and outflow fractions over the following range:

$$-3 \leq \log C_{\rm eff} \leq +1$$
$$0 \leq B_{\rm out} \leq 0.7.$$

For every choice of parameters, the $I-K'$ color of the unnormalized composite spectral energy distribution is used in order to find the absolute luminosity using the color-magnitude relation of the sample of Verheijen (1997):

$$M'_K = -\frac{(I-K')+1.417}{0.1304}, \qquad (7)$$

which is shown as a solid line in the inset of Figure 1. The color-magnitude relation found by de Grijs & Peletier (1999) from a subsample of the Surface Photometry Catalogue of ESO-Uppsala galaxies is shown as a dashed line, in remarkable agreement with the fit from the sample of UMa galaxies. In fact, the universality of the color-magnitude relation in disk galaxies is explored by de Grijs & Peletier (1999) as a plausible distance indicator, with accuracies deemed to be better than 25 %.

Once the spectral energy distribution is normalized, we can compare the predicted Tully-Fisher relations in different wavebands with the observations. Table 1 shows the result of fitting the photometry of disk galaxies in the Ursa Major cluster (Verheijen 1997) to a Tully-Fisher relation in different filters ($X = \{B,R,I,K'\}$):

$$M_X^{\rm TF} = \alpha_X \log v_{\rm ROT} + \beta_X. \qquad (8)$$

We perform a two-stage linear fit with a first estimate of the slope and zero point by applying absolute deviations. This first estimate is used to remove points which lie more than one standard deviation off the linear fit. A least squares fit is subsequently applied to the remaining points. This technique prevents outliers from contributing significantly to the fit. These fits allow us to estimate how well different star formation histories — described by the parameters — can account for the observed Tully-Fisher relations in different passbands. We define a χ^2 by:

$$\chi^2 \equiv \Sigma_{X=\{B,R,I,K'\}} \frac{(M_X - M_X^{\rm TF})^2}{\sigma_X^2}. \qquad (9)$$

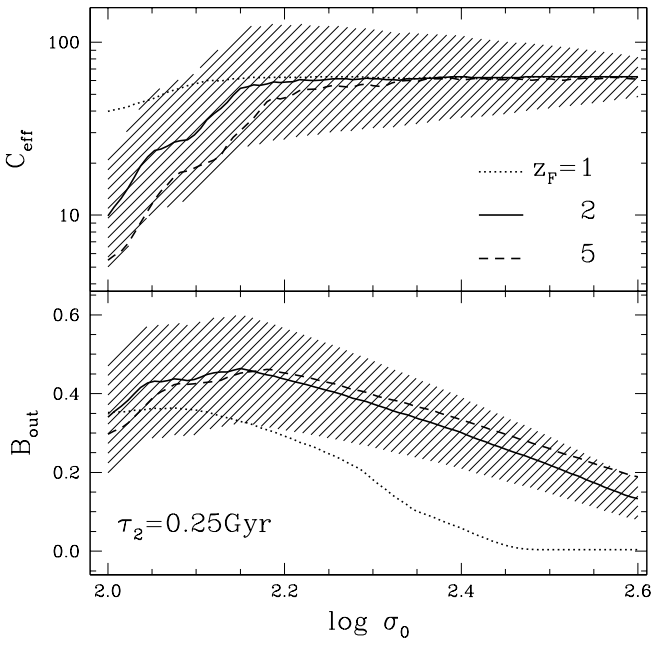

FIG. 6.— Range of star formation efficiencies (*top*) and gas outflows (*bottom*) as a function of central velocity dispersion (σ_0) that give the best fit to the chemical enrichment model constrained by the Faber-Jackson relation observed in Coma elliptical galaxies in $\{U,V,J,{\rm and}K\}$ bands. The shaded area represents the 90% confidence levels of the χ^2 analysis performed for the $z_F = 2$ model.

Figures 4 and 5 show the range of star formation efficiencies and outflow fractions, respectively, allowed by the observed photometry. This range is shown in four panels corresponding to four different infall timescales (i.e. four different galaxy types). Each panel gives the result for three different formation redshifts (thick lines) using a linear Schmidt law ($n = 1$ in equation 3). The result for a quadratic law ($n = 2$) is shown for $z_F = 2$ as a thin solid line. The 90% confidence level of the χ^2 fit for $z_F = 2$ and $n = 1$ is shown as a shaded area in Figure 4 and as error bars in Figure 5.

5. HOW EFFICIENT IS STAR FORMATION ?

Figures 4 and 5 show that a very large range of star formation efficiencies is needed in order to explain the observations, whereas outflows seem to be unimportant in disk galaxies. Over a velocity range of $\Delta \log v_{\rm ROT} = 0.6$ dex we find a range of star formation efficiencies corresponding to gas-to-star processing timescales that span over 2 decades between very small disks ($v_{\rm ROT} \sim 100$ km s^{-1}) and massive ones ($v_{\rm ROT} \sim 400$ km s^{-1}) for various infall parameters. This result is very robust given the assumptions and the model presented here, as well as the 90% confidence level of our χ^2 fit. While outflows could play a role, these cannot be very important. The error bars shown in Figure 5 show that outflows in low-mass systems cannot be larger than 20%. Furthermore, a constant value $B_{\rm out} \sim 0$, regardless of $v_{\rm ROT}$, is also consistent with the data. This is also in agreement with the negligible effect of supernova-driven winds in disks as found in hydrodynamic simulations (MacLow & Ferrara 1999). The correlation between $C_{\rm eff}$ and $v_{\rm ROT}$ does not change significantly with respect to morphological type (roughly described by our infall timescale τ_2). This is in agreement with Young et al. (1996) who find no variation in the global ratio $L(H\alpha)/M(H_2)$ for spiral galaxies with types Sa-Sc.

TABLE 1

Fits to the Tully-Fisher relation: $M_X^{\rm TF} = \alpha_X \log v_{\rm ROT} + \beta_X$, and scatter σ_X

Band (X)	α_X	β_X	σ_X
B	−6.387	−3.842	0.370
R	−7.356	−2.284	0.348
I	−8.020	−1.061	0.394
K'	−9.368	+0.849	0.323

The range of efficiencies is consistent with the observations of Kennicutt (1998b), who defines an efficiency with respect to surface densities: $A \equiv \Sigma_\psi / \Sigma_{\rm gas}^n$. The data fit a power law index $n = 1.4 \pm 0.15$, with the efficiency ranging over a factor of 100. However, the observed efficiencies are systematically one order of magnitude higher than our $C_{\rm eff}$, with the lowest value around $A \sim 0.1$ (thereby the gas consumption timescales $A^{-1} \lesssim 10$ Gyr are significantly shorter than $C_{\rm eff}^{-1}$). There are various reasons for such a discrepancy between A and $C_{\rm eff}$. We believe the most important one to be a systematic underestimate of the amount of molecular hydrogen, which we discuss in more detail in the next sections. Furthermore, the star formation rates obtained from $H\alpha$ measurements are corrected for extinction by a factor of 2.8 using a comparison between $H\alpha$ fluxes and radio fluxes due to free-free emission at 3 and 6 cm (Kennicutt 1983). However, the radio emission is assumed to be purely thermal. A non-thermal contribution in the radio fluxes would imply a systematic overestimate of the star formation rates, with a corresponding increase of A with respect to $C_{\rm eff}$. Additionally, a universal star formation threshold in the surface gas density would result in lower integrated efficiencies — such as the parameter $C_{\rm eff}$ — compared to surface-based measurements such as A, with the correction factor roughly amounting to the ratio of the disk area over which the surface mass density is above threshold with respect to the total area of the galaxy. A linear Schmidt law and a surface density threshold for the star formation (Σ_{th}) would imply:

$$\psi(t) = C_{\rm eff} M_g(t) = A \int d^2 r \Sigma_g(r,t) \Theta\Big(\Sigma_g(r,t) - \Sigma_{th}\Big) < A M_g(t), \tag{10}$$

where $\Theta(x)$ is the step function. For an exponential density profile with scale-length h, i.e. $\Sigma(r) = \Sigma_0 \exp(-r/h)$ we find:

$$C_{\rm eff} = A\Big(1 - e^{-x_0}\Big) < A, \tag{11}$$

such that $\Sigma(r = x_0 h) = \Sigma_{th}$. Hence, a threshold will cause a systematic offset towards lower values for the integrated star formation efficiencies. A delay in the galaxy formation process can also yield higher star formation efficiencies. The dot-dash line in the bottom-left panel of Figure 4 gives the star formation efficiencies predicted for $z_F = 0.3$, which are about one order of magnitude higher than those for models with $z_F \geq 1$. However, this implies the bulk of the stellar populations should have ages $\lesssim 2.5$ Gyr, which leads to a drastic change of the luminosity function of disk galaxies at moderate redshift that is not seen (e.g. Lilly et al. 1995).

The large range of star formation efficiencies shown in Figure 4 is in remarkable contrast with the region of parameter space allowed by the color-magnitude constraint in early-type systems. The photometry of spheroids is compatible with either a large range of star formation efficiencies *and/or* a wide range of gas ejected in outflows (Ferreras & Silk 2000b). In fact, the lack of evolution of the slope of the color-magnitude relation of early-type galaxies with redshift suggests the mass sequence of early-type galaxies is a pure metallicity sequence, where the stellar populations have roughly similar ages regardless of galaxy mass so that the color range observed is explained by a mass-metallicity correlation. Such a correlation, without a similar mass-age connection, can only be explained by assuming outflows are very important in low-mass systems. In order to test our model, we applied the same chemical enrichment code and fitting technique to the Faber-Jackson relation in early-type systems. We used the U, V, J and K photometry of elliptical galaxies in the Coma cluster from Bower, Lucey & Ellis (1992). The best fits are shown in Figure 6 for the star formation efficiency (*top*) and outflow fraction (*bottom*), taking a linear Schmidt law and three different formation redshifts: $z_F = \{1, 2, 5\}$. We chose a short infall timescale: $\tau_2 = 0.25$ Gyr, although larger values were also used, leading to similar results for $\tau_2 = 0.5$ and 1 Gyr. Longer infall timescales were incompatible with the photometric data. The shaded area represents the 90% confidence level of the χ^2 fit in the $z_F = 2$ case. In contrast to disk galaxies (Figures 4 and 5), early-type systems require very high star formation efficiencies, and are compatible with a significant correlation between galaxy mass and fraction of gas ejected in outflows. This is in agreement with the enhanced star formation efficiencies observed in mergers (Young et al. 1996), which are believed to be associated with the process of spheroid formation. A plausible scenario to reconcile these two very different trends is that disk galaxies are dynamically "ordered" systems, where gas ejection can only take place through feedback from supernovae, whereas early-type galaxies (or disk bulges) have a more complicated dynamical history, which can allow for a significant amount of gas (and metals) being ejected from the galaxy, as expected in dwarf galaxy mergers (Gnedin 1998). Furthermore, this process should be correlated with the mass of the galaxy (i.e. more gas being ejected in events involving less massive mergers).

6. OF GAS AND STARS

The large range of star formation efficiencies required by our model — shown in Figure 4 — implies that there is a large difference in gas content with respect to galaxy luminosity. As a rough approximation, the inverse of the star formation efficiency gives the timescale for the processing of gas into stars (in Gyr). We can see in the figure that in the interval $2.1 < \log v_{\rm ROT} < 2.6$ — which corresponds to a range of 4.5 magnitudes in absolute K-band luminosity — $C_{\rm eff}$ spans two orders of magnitude. This means it takes 100 times longer to

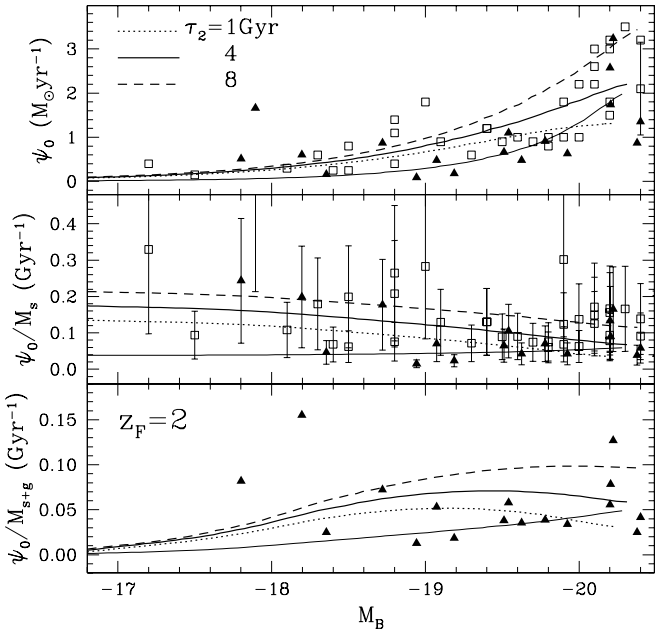

FIG. 7.— Star formation rates at zero redshift: The model predictions are compared against the samples of Kennicutt (1983; squares) and Kennicutt (1994; triangles). The thick dotted, solid and dashed lines correspond to a linear Schmidt-type law with different infall timescales (τ_2 = 1, 4 and 8 Gyr, respectively). The thin solid line is the result for a quadratic Schmidt-type law. The top, medium and bottom panels compare the absolute; specific-weighted-by-stars, and specific-weighted-by-total-mass star formation rates, respectively. The conversion from *B*-band absolute luminosity (from the data) to stellar mass is done by assuming a range in mass-to-light ratios between $-0.15 < \log(M/L_B) < +0.15$, predicted by population synthesis models for a large range of star formation histories. The points in the bottom panel includes an estimate of the mass in molecular hydrogen using CO as tracer.

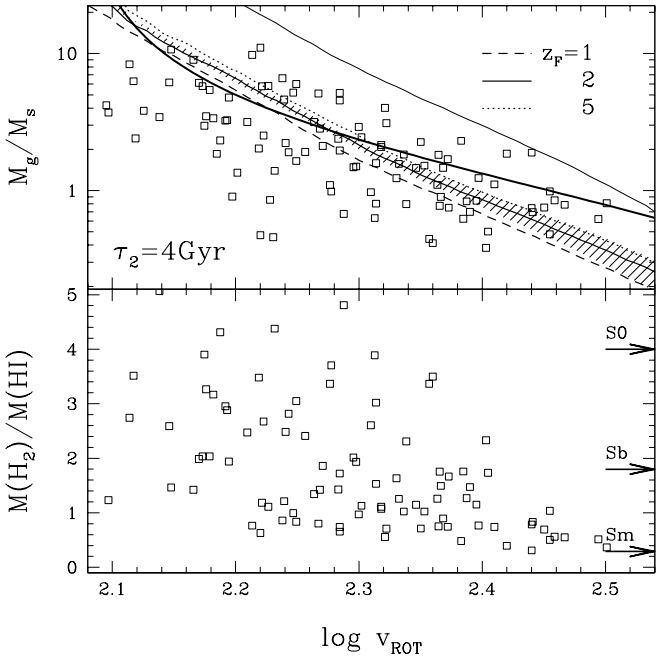

FIG. 8.— *Top panel:* Gas-to-stellar mass fractions predicted by the model at three different formation redshifts (linear Schmidt law for τ_2 = 4 Gyr as dashed, solid and dotted lines for z_F = 1, 2, and 5, respectively; thin solid line for τ_2 = 4 Gyr, z_F = 2 for a quadratic Schmidt law). The shaded region gives the range of gas fractions at z_F = 2 for $1 < \tau_2/\mathrm{Gyr} < 8$. The points are from McGaugh et al. (2000), after being corrected so that the stellar masses correspond to *K*-band luminosities that obey the Tully-Fisher relation. The thick line is the fit-by-eye of Bell & de Jong (2000) for the mass fractions found in a sample of low-inclination spiral galaxies (see text for details). *Bottom panel:* If we take the model predictions at face value, one has to consider the presence of molecular hydrogen. The points give the expected ratio of molecular to atomic hydrogen for the sample shown above. A rough upper limit to the gas fraction — given by the rotation curves for a maximal disk — is ~ 6 (Combes 2000). The arrows are the results from Young & Knezek (1989) as a function of galaxy morphology.

process stars in the faintest disk galaxies. Furthermore, the gas mass fraction: $f_g \equiv M_g/(M_g + M_s)$, where M_g and M_s are the mass in gas and stars, respectively, will also vary over a very large range. As a simple example, we can write the gas mass fraction in a closed-box model (using $f(t) = \delta(t)$ in equation 4) as:

$$f_g(t) = \exp(-t/\tau_g), \tag{12}$$

with the star-processing timescale (τ_g) defined in (5). Massive systems have efficiencies close to $C_{\rm eff} \sim 1$, i.e. $\tau_g \sim 1$ Gyr, which means the gas mass fraction should be very low in disk galaxies at $z = 0$. However, low-mass galaxies are predicted to have $\tau_g \sim 100$ Gyr, which boosts the gas mass fraction in local galaxies up to 90%. Hence, galaxies with low rotation velocities should have large amounts of gas. This issue is hard to circumvent by redefining the model: the index of the Schmidt power law used in the correlation between gas mass and star formation rates does not change the range of efficiencies. We also considered several other models with a time-varying star formation efficiency but the final results were very similar to those presented here.

Figure 7 checks the consistency of our model with estimates of star formation in nearby spiral galaxies using the flux of the Hα emission line as the observable. The data points are from Kennicutt (1983, squares; 1994, triangles). The top panel plots the prediction of the absolute star formation rate (in $M_\odot \mathrm{yr}^{-1}$) as a function of *B*-band absolute luminosity for three different infall timescales: $\tau_2 = \{1, 4, \text{and } 8\}$ Gyr, using a linear Schmidt law. The thin solid line is the prediction for τ_2 = 4 Gyr for a quadratic law. A typical error bar from the data is also shown. The star formation rates obtained from these measurements can have uncertainties mainly due to variable extinction up to $\pm$50%. The model predictions show that even though there is not much gas in larger mass systems, their high star formation efficiencies account for an increase in the SFR with luminosity.

Table 2 gives the fits to the star formation rate as a function of stellar mass ($\psi \propto M_s^b$) predicted by the model, for various infall parameters. The power law index lies in the range $b \sim 0.7 - 0.8$ and as expected, it varies more with formation redshift for shorter infall timescales. The middle panel of Figure 7 shows the specific star formation rate weighted by stellar mass (ψ/M_s), which decreases with increasing mass since $b < 1$. In order to transform the absolute luminosities from Kennicutt (1983; 1994) to stellar masses, we assume a large range in mass-to-light ratios $-0.15 < \log(M/L_B) < +0.15$ in order to account for different age distributions or initial mass functions of the stellar component. The error bars shown give the range of specific star formation rates depending on the mass-to-light ratio chosen. Finally, the bottom panel plots the specific star formation rate weighted by total (baryonic) matter, i.e. stars and gas. In this case only Kennicutt (1994) gives gas masses. Both atomic and molecular hydrogen are considered and helium is included by correcting the final mass by a factor of 1.4. The data is consistent with the model predictions, except for the two faintest data points, which appear to be in disagree-

ment with such a high gas content. One explanation for this is that the molecular hydrogen measured has been underestimated. Molecular hydrogen is usually measured indirectly, by assuming a constant H_2/CO ratio. Systems with lower metallicities than the galaxies used to calibrate this ratio should have larger H_2 masses than the estimates according to this technique (Combes 1999). The bottom panel of Figure 8 also shows the results from Young & Knezek (1989) regarding the dependence of $M(H_2)/M(HI)$ with morphology, where the detection of H_2 is based on CO observations. The observed trend, which finds more molecular hydrogen in earlier types (which have higher metallicities), is a reflection of the strong dependence of the H_2/CO ratio with metal abundance.

In order to explore this point further, we used the data presented by McGaugh et al (2000) who motivated the existence of a baryon-dominated Tully-Fisher relation, i.e. a tight correlation between total stellar+gas mass and rotational velocity. They inferred the stellar masses from photometric data in optical (I) and near infrared (H and K') bands, by assuming a fixed mass-to-light ratio (however, see Bell & de Jong 2001). Near infrared observations are usually good stellar mass observables since M/L_K does not change much over a large range of ages. For consistency, we decided to use the Tully-Fisher relation as a constraint so that the stellar masses were corrected to abide by the linear fits shown in Table 1. The gas-to-stellar ratios are shown in Figure 8 along with model predictions for three formation redshifts for a linear Schmidt law and also for a prediction using a quadratic law. The gas fractions predicted for the quadratic Schmidt law are higher since such a model requires even lower star formation efficiencies at the faint end (Figure 4).

The figure also shows the fit-by-eye from Bell & de Jong (2000) who estimated the gas fraction to be: $f_g = M_g/(M_g + M_s) = 0.8 + 0.14(M_K - 20)$ in a sample of low-inclination spiral galaxies. The fractions were computed from K-band luminosities (in order to find stellar masses) and H I fluxes corrected to include helium. They also included the contribution from molecular hydrogen by using the ratio of molecular to atomic gas masses as a function of morphological type (Young & Knezek 1989). Our models are thereby consistent with the data for a linear Schmidt law. However, the large scatter observed could be associated with the presence of undetected molecular hydrogen. The bottom panel shows the ratio between molecular and atomic hydrogen predicted if we take the models at face value. It is interesting to notice that a larger amount of undetected H_2 is expected for fainter galaxies, in agreement with the fact that fainter galaxies have low efficiencies which translate into lower average metallicities (cf fig. 2) so that the H_2/CO ratio used to trace H_2 could be in significant disagreement with the calibrations (Combes 2000).

The ratios shown in the figure are still consistent with the total amount of matter to be expected from the rotation curves of spirals. Combes (1999) showed that using a ratio of $M(H_2)/M(HI) \sim 6.2$, the gas and stellar content in NGC 1560 can account for the rotation curve out to 8 kpc. Furthermore, observations by Valentijn & Van der Werf (1999) of the lowest pure rotational lines of H_2 in NGC 891 out to 11 kpc, using the Short-Wavelength Spectrometer on board the Infrared Space Observatory, found large amounts of H_2 at temperatures $T \sim 80-90$ K, outweighing H I by a factor $5-15$. More data is clearly needed to draw a definitive conclusion about the presence of a high mass in molecular hydrogen. Nevertheless, the agreement between these observations and our model predictions — arising from the need for very low star formation efficiencies in low-mass galaxies — motivates further exploration of this problem, especially given the impact that such an issue has on galaxy formation as well as on our understanding of the properties of dark matter.

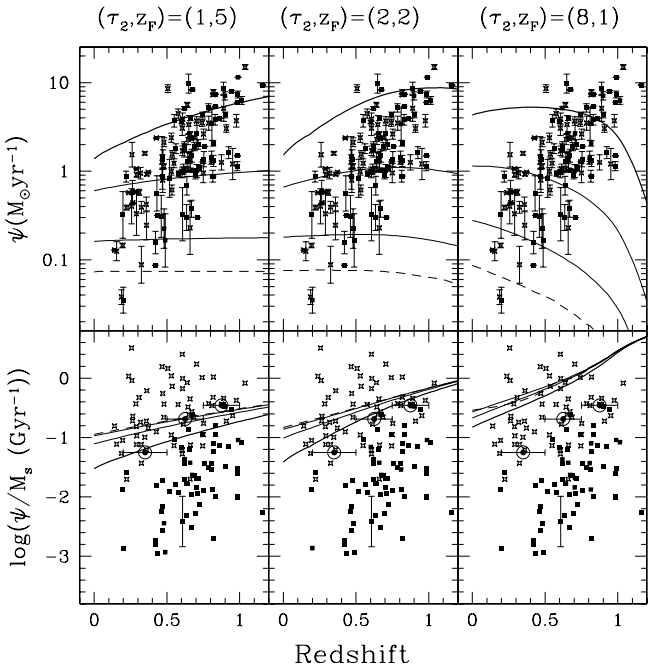

FIG. 9.— Redshift evolution of the absolute (*top*) and specific star formation rate weighted by stellar mass (*bottom*), for a set of rotational velocities: The curves correspond to $\log v_{ROT}$ = 2.6, (thick) 2.4, 2.2 and 2.0 (dashed line). The infall parameters $(\tau_2/\mathrm{Gyr}, z_F)$ are shown on top. The data points are from the sample of Brinchmann (1999). The error bars come straight from observational uncertainties of [O II] emission, used as tracer of star formation. The sample has been divided with respect to stellar mass at the median ($\log(M_s/M_\odot) = 10.3$), with high-mass galaxies represented as filled squares. In the bottom panels we only show one typical error bar for clarity purposes. The circles with horizontal error bars give the best fit for the specific star formation rate at $\log(M_s/M_\odot) = 10$ found by Brinchmann & Ellis (2000) in three redshift bins over the redshift range represented by the error bars.

We want to emphasize that a possible weakness in the model presented here is the *absolute* estimate of star formation efficiencies. One should take the values of C_{eff} as lower bounds for a given galaxy if the results are to be compared with local efficiencies defined as $A \sim \Sigma_\psi/\Sigma_g^n$, where Σ_g and Σ_ψ are the surface densities of gas and star formation rate, respectively. However, even this method of estimating efficiencies is questionable after the discovery of star formation in the extreme outer regions of disk galaxies, which cannot be described by a single-component Schmidt law (Ferguson et al. 1998). The stellar metallicities predicted by our model for rotation velocities corresponding to a Milky Way sized galaxy (which implies $0.1 \lesssim C_{\mathrm{eff}} \lesssim 0.2$) are in the right ballpark: $-0.1 < [\mathrm{Fe/H}] < +0.05$, whereas low efficiencies $C_{\mathrm{eff}} \sim 0.01 - 0.02$ predicted by the model for a galaxy like the Large Magellanic Cloud ($M_B = -18$) give metallicities ($-1.1 < [\mathrm{Fe/H}] < -0.8$) that are consistent with the observations of the young clusters — with ages $t \lesssim 3$ Gyr — with the lowest metallicities (Olszewski, Suntzeff & Mateo 1996). However, notice the large range of metallicities found in old LMC clusters ($-2.1 < [\mathrm{Fe/H}] < -1.4$ for $t \sim 14$ Gyr) which hints at a more complicated star formation history.

TABLE 2

Star Formation Rates: $\log(\psi/M_\odot yr^{-1}) = \mathcal{A} + b\log(M_s/M_\odot)$

τ_2/Gyr	z_F	b	$\mathcal{A}$
1	1	0.665	–6.763
	2	0.716	–7.311
	5	0.741	–7.597
4	1	0.796	–7.817
	2	0.795	–7.937
	5	0.796	–8.018
8	1	0.859	–8.311
	2	0.862	–8.449
	5	0.862	–8.532

7. EVOLUTION OF THE TULLY-FISHER RELATION WITH REDSHIFT

The star formation histories given by the best fits to the efficiency and the fraction of gas in outflows shown in Figures 4 and 5 can be used to evolve the systems backwards in time. A major consequence of the large range in star formation efficiencies found with respect to rotational velocity is that low-mass systems will have a broader distribution of stellar ages. This implies a stronger evolution in luminosity with lookback time. Furthermore, a low efficiency will yield a constant and low star formation rate with redshift. On the other hand, massive galaxies will undergo milder changes in absolute luminosity because of their high star formation efficiencies, and this will narrow the expected age distribution (cf. Fig. 3). The star formation rate for massive galaxies, however, experiences a significant increase with redshift. Figure 9 illustrates this point: model predictions of the redshift evolution of the absolute (*top*) and specific weighted-by-mass (*bottom*) star formation rates are shown for $\log v_{\rm ROT} = \{2.6$ (thick line), $2.4, 2.2,$ and 2.0 (dashed)$\}$. An increase in the specific star formation rate with decreasing mass is predicted, spanning a factor of 4 in ψ/M_s between $\log v_{\rm ROT} = 2.0$ and 2.6, i.e. roughly linear with $v_{\rm ROT}$. This difference in ψ/M_s gets narrower at high redshifts, explained by the fact that the increase in the specific SFR in galaxies with a high efficiency will evolve faster with lookback time, whereas low-mass systems — with low values of $C_{\rm eff}$ — feature a low and nearly constant SFR.

The estimates of stellar mass and star formation rates of a sample of field galaxies from the Canada France Redshift Survey and from the Hubble Deep Field North and its flanking fields are also shown in Figure 8 (Brinchmann 1999). The sample spans a wide redshift range ($0.2 < z < 1$). The stellar masses are obtained following *K*-band luminosities, but adding a correction term based on a comparison between multiband optical photometry and population synthesis models for various ages, metallicities and dust extinction values (Brinchmann & Ellis 2000). These authors estimated the uncertainties in the computation of the stellar mass to be $\log \Delta M_s \sim 0.3$ dex. The ongoing star formation rate is computed from the flux of the [O II] emission line. The sample is divided in Figure 8 with respect to stellar mass, so that galaxies with masses larger (smaller) than the median ($\log(M_s/M_\odot) = 10.3$) are represented by squares (stars). The bottom panels only show one typical error bar to avoid crowding the figure. Taking the model predictions at face value, one would explain the lack of data points in the bottom right portion of the top panels by a selection bias of the sample which would have to be missing systems with low rotational velocities (or faint absolute luminosities) at high redshift. It is also interesting to notice that the region with $\psi \gtrsim 5 M_\odot {\rm yr}^{-1}$ is mainly populated by massive galaxies. Brinchmann & Ellis (2000) find a significant increase in the specific star formation rate with redshift, shown in the bottom panels of Figure 9 as big circles with error bars. The points are the values at $\log(M_s/M_\odot) = 10$ of the best fit found in the redshift bins represented by the horizontal error bars. The values for higher (lower) mass systems will roughly shift linearly to lower (higher) specific SFRs. Hence, this fits into our model by assuming a correlation between stellar mass and infall parameters, so that galaxies with more extended star formation histories should correspond to low-mass systems and vice versa.

The redshift evolution of the Tully-Fisher relation is another interesting issue which becomes possible to quantify with recent observations of the rotation curves of disk galaxies at moderate and high redshift (Vogt et al. 1997). The power of an analysis including star formation lies in the ability to predict relative changes in luminosity evolution caused by a different age distribution of the stellar populations. In contrast to semi-analytic modellers who are more concerned with the evolution of the zero point of the Tully-Fisher relation, we can "turn the crank" of our model — which is constrained at zero redshift by the local Tully-Fisher relation — backwards in time and find luminosity changes as a function of galaxy mass. Figure 10 shows that even more importantly than the zero point, *the slope* (γ, with $L \propto v_{\rm ROT}^\gamma$) of the Tully-Fisher relation is a crucial parameter to explore. The panels show the evolution of several properties in optical (*B*; left) and near infrared (*K*; right) passbands. The bottom panels show the predicted evolution of $\gamma_{B,K}$ for $\tau_2 = 4$ Gyr and three formation redshifts using a linear Schmidt law, and for $z_F = 2$ with a quadratic law (dashed-dotted line). The shaded areas in all panels give the predictions at $z_F = 2$ when allowing a wide range of infall timescales ($1 < \tau_2/{\rm Gyr} < 8$). The steepening of the slope is a consequence of the very low star formation efficiencies at the low-mass end, which imply a broader distribution of stellar ages. Models based on simple arguments of structure formation fail to include the effect of the evolution of the stellar populations. Hence, the prediction of Mo, Mao & White (1998), who tie the evolution of the luminous component in disks to the parameters defining the dark matter halo in which they are embedded, uses a scaling argument to find a constant $\gamma = 3$, obviously regardless

of passband and therefore inconsistent with the observations.

A slope change implies that the measured zero point will depend on the absolute luminosity considered. The top panels plot the luminosity evolution for systems with a rotational velocity of 100 km s^{-1}, whereas the middle panels correspond to massive galaxies, with $\log v_{\rm ROT} = 2.6$. As expected, more massive disks undergo a milder luminosity evolution. Recent observations at moderate and high redshift are shown as well. The latest work of Vogt et al. (2000; filled squares) on disks in the Groth Survey Strip, extending over a large redshift range: $0.2 < z < 1$, shows a very small — if any — evolution in absolute B-band luminosity ($\Delta M_B \lesssim -0.2$). The observations of Bershady et al. (1999; hollow squares) at $z \sim 0.4$ hint at a slightly different luminosity evolution depending on rest frame $B-R$ color, which we coarsely map into $\log v_{\rm ROT}$. Hence, low-mass systems are found to have $\Delta M_B = -0.5 \pm 0.5$ whereas massive disks appear not to have any significant evolution: $\Delta M_B = 0.0 \pm 0.5$. This result is in good agreement with the model, which gives a larger luminosity evolution for low-mass disks. The triangle represents the result from Simard & Pritchet (1998), who find very strong evolution ($\Delta M_B \sim -2$) in a sample of strong [O II] emitters at $z \sim 0.35$, in remarkable contrast with the other observations as well as with our model. One could speculate that disks with a star formation rate peaked at $z_F \sim 0.5-1.0$ could in principle explain this last data point, assuming that the selection criterion biased the sample towards systems with a very recent star formation history.

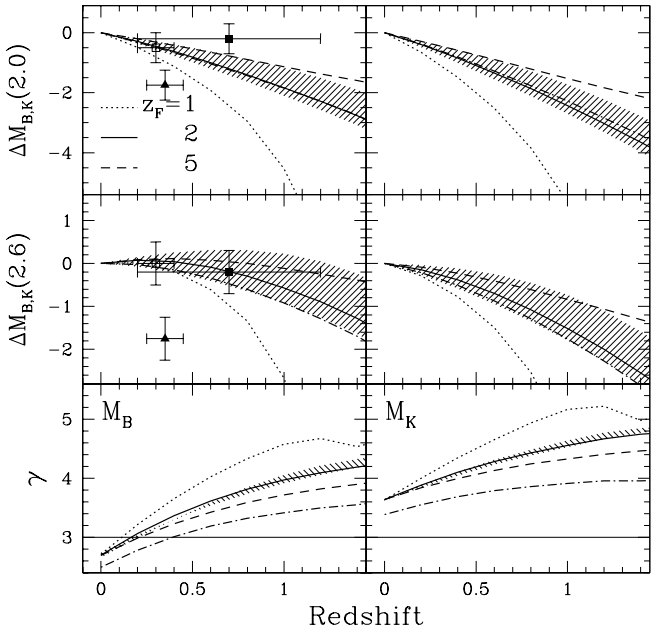

FIG. 10.— Redshift evolution of the Tully-Fisher relation. The evolution with redshift of the zero points at $\log v_{ROT} = 2$ (*top panels*) and 2.6 (*medium panels*) are shown as well as the change in slope γ ($L \propto v_{ROT}^{\gamma}$) in optical ($B$; *left*) and near-infrared bands (K; *right*). The thick dotted, solid and dashed lines correspond to formation redshifts of $z_F = 1, 2$ and 5, respectively, and all three lines assume an infall timescale $\tau_2 = 4$ Gyr and a linear Schmidt law. The predictions for a quadratic law, with $\tau_2 = 4$ Gyr and $z_F = 2$ are shown as a dash-dot line. The shaded area gives the predictions for a range in infall timescales, between $\tau_2 = 1$ and 8 Gyr at $z_F = 2$. The points show the offset of the Tully-Fisher relation in rest frame B band, in observations at moderate and high redshift from Bershady et al. (1999; hollow square); Vogt et al. (2000; filled square), and Simard & Pritchet (1998; triangle). The horizontal error bar just encompasses the redshift range of the observations. In the bottom panels, the horizontal line at $\gamma = 3$ shows the prediction of a simple dynamical model that does not consider the evolution of the stellar populations (e.g. Mo, Mao & White 1998).

8. DISCUSSION

In this paper we have presented a phenomenological approach to galaxy formation which reduces the process of star formation to a set of a few parameters controlling the infall of primordial gas, the efficiency of processing gas to form stars, and the fraction of gas and metals that are ejected from the galaxy. These parameters are not set *a priori*. Instead, they are allowed to vary over a large volume of parameter space. The Tully-Fisher (1977) relation in different wavebands is used as a constraint, in order to find the parameter space compatible with the data. Our results show that gas outflows should not play a major role in explaining the color and luminosity range of disk galaxies, whereas a very large range of star formation efficiencies ($C_{\rm eff}$) is required. A power law fit to the correlation between $C_{\rm eff}$ and rotational velocity ($v_{\rm ROT}$) gives a slope $\Delta \log C_{\rm eff} / \Delta \log v_{\rm ROT} \sim 4$ regardless of either the infall parameters chosen or the exponent used in the Schmidt law relating gas density and star formation rates (see Figure 4). For a range of rotational velocities $2.1 < \log v_{\rm ROT} < 2.6$ — which maps into a 4.5 mag range in absolute K-band luminosity — we therefore predict a star formation efficiency variation of around 2 orders of magnitude. This corresponds to star processing timescales which are 100 times longer for low-mass disks compared to the bright ones. In contrast, Bell & Bower (2000) suggest a mass dependency of either infall or outflows in order to explain the observations, although their models did not allow for a wide range of star formation efficiencies. Moreover, Boissier et al. (2001) found no correlation between the star formation efficiency and the galaxy mass, using a chemo-spectrophotometric evolution model calibrated on the Milky Way and extended to a wide range of galaxy masses. However, the observed color range must be accounted for by a large range of formation redshifts, so that massive disks are formed *earlier* than less massive ones. The predicted large variation in stellar ages as a function of galaxy mass may be in conflict with the redshift evolution of both the luminosity function of disk galaxies and the Tully-Fisher relation. If we impose on our models formation redshifts $z_F \gtrsim 1$ for all galaxy masses, a large range of efficiencies are predicted. Furthermore, a hierarchical scenario — for which small structures collapse first — would increase the slope of the correlation between $C_{\rm eff}$ and rotation velocity. The departure of the scaling behavior of the star formation efficiency found in this paper with respect to dynamical back-of-the-envelope estimates frequently used in semi-analytic modelling, i.e. $C_{\rm eff} \propto t_{dyn}^{-1} \propto v_{\rm ROT}^3 / M$, where t_{dyn} is a characteristic dynamical time-scale for the galaxy (eg. Kauffmann, White & Guiderdoni 1993), shows that the Tully-Fisher relation cannot be fully explained by the properties of the halo, but rather, needs a component incorporating self-regulated star formation (Silk 1997, 2000).

We also applied our model using the Faber-Jackson (1976) correlation in spheroids as a constraint, finding a rather constant and high efficiency and a significant range in gas outflows. This behavior could be explained by the different dynamical history of disks and spheroids. Early-type systems have undergone mergers with equal mass progenitors, which can drive a significant amount of gas out of galaxies. On the other hand, the standard framework for disk galaxy formation assumes smooth infall and cooling of gas on to the centers of dark matter halos. Furthermore, the low outflow fractions found in disks for

any galaxy mass enable us to reject supernova-driven winds as an important mechanism for driving gas and metals out of the interstellar medium of galaxies, in agreement with the hydrodynamic simulations of McLow & Ferrara (1999) and the modelling of star formation in dwarf galaxies by Ferrara & Tolstoy (2000).

The large range of star formation efficiencies obtained by our model implies that low-mass galaxies should have a large fraction of baryonic matter in the form of gas. As a sanity check, we compared the predictions for the star formation rate at $z = 0$ as a function of stellar mass with Kennicutt (1983; 1994) and found good agreement. A fit to a power law — $\psi \propto M_s^b$ — gives an exponent $b \sim 0.7-0.8$ for a large range of infall parameters (Table 2). Hence, in the tug-of-war between star formation efficiency and galaxy masses, the former wins over, giving higher star formation rates in brighter galaxies. In a speculative mode, we suggest that a large fraction of the considerable amounts of gas predicted for systems with low efficiencies could be in cold molecular hydrogen, a rather elusive component. In the bottom panel of Figure 8 we took our model at face value and compared it with the stellar and gas content (atomic hydrogen plus helium) from the sample compiled by McGaugh et al. (2000), and we inferred a significant increase in the ratio of molecular to atomic hydrogen for less massive galaxies. This can be accounted for if there is a significant offset in galaxies with low metallicities from the usual H_2 to CO conversion factor used to detect molecular hydrogen (Combes 2000). Using a direct technique to search for H_2, large amounts of not-too-cold molecular gas ($T \sim 80-90$ K) have been detected through the lowest pure rotational transitions in NGC 891 (Valentijn & Van der Werf 1999). Incidentally, an extrapolation of up to $M(H_2)/M(HI) \sim 6.2$ can account for the rotation curves of disks (Combes 1999). This issue has important implications not only for galaxy formation but also for cosmology: the existence of such large amounts of H_2 on galaxy scales could favor a parameter space of dark matter with partially suppressed hierarchical galaxy formation on sub-galactic scales, as a consequence of the enhanced free streaming lengths found in scenarios such as warm dark matter (e.g. Colín, Avila-Reese & Valenzuela 2000; Bode, Ostriker & Turok 2000). We remark that the large range in star formation efficiencies should be incorporated into models of galaxy formation. Semi-analytical simulations of galaxy formation which assume a constant star formation efficiency as a function of circular velocity (Lacey & Silk 1991; White & Frenk 1991; Cole et al. 2000; Kauffmann et al. 1999; Somerville & Primack 1999) are far too simplistic to give meaningful predictions of, for example, the cosmic star formation history.

We used our model to infer the redshift evolution of star formation and of the Tully-Fisher relation. Star formation rate predictions are compatible with the data, although the scatter, uncertainties and various biases makes this a rather uncertain endeavor. SFRs are expected to undergo stronger evolution in systems with high rotational velocities, whereas low-mass systems feature a steadier formation rate due to their low efficiencies. The range of specific formation rates with stellar mass is predicted to decrease with redshift. The Tully-Fisher relation is expected to evolve *in slope*, as well as in zero point, because the age distribution of the stellar population varies with galaxy mass, being more spread out in low-mass disks. Hence, we expect a steepening of the slope. For instance, in rest frame B band the slope changes from $\gamma_B \sim 3$ at zero redshift ($L \propto v_{\rm ROT}^{\gamma}$) up to $\gamma \sim 4-4.5$ at $z \sim 1$ (Figure 10), with a slight dependence on the formation redshift, giving stronger evolution for low formation redshifts. The zero point should thus be given with respect to some fiducial rotational velocity. We show the evolution of the zero point at low ($\log v_{\rm ROT} = 2$) and high mass (2.6) is in agreement with the latest observations from Vogt et al. (2000) for high mass systems, as well as with Bershady et al. (1998) both for high and low masses. Notwithstanding the many observational difficulties that complicate accurate estimates of the redshift evolution of γ, we find the evolution of the slope of the Tully-Fisher relation to be the best observable for exploring the star formation process in disk galaxies, in analogy with the study of the slope of the fundamental plane in early-type systems (Ferreras & Silk 2000b).

ACKNOWLEDGMENTS

IF is supported by a grant from the European Community under contract HPMF-CT-1999-00109. We would very much like to thank Jarle Brinchmann for helpful discussions and for making available the data from his PhD thesis. We would also like to thank Eric Bell and Stacy McGaugh for providing their data on disk gas masses. The anonymous referee is gratefully acknowledged for useful comments and suggestions.

REFERENCES

Baugh, C. M., Cole, S., Frenk, C. S. & Lacey, C. G. 1998, ApJ, 498, 504
Bell, E. F. & Bower, R. G. 2000, MNRAS, 319, 235
Bell, E. F. & de Jong, R. S. 2000, MNRAS, 312, 497
Bell, E. F. & de Jong, R. S. 2001, ApJ, March 20, astro-ph/0011493
Bershady, M. A., Haynes, M. P., Giovanelli, R. & Andersen, D. R. 1999, in Merritt, D. R., Valluri, M. & Sellwood, J. A., eds, ASP Conf. Ser. 182, Galaxy Dynamics. Astron. Soc. Pac., San Francisco, p. 499
Bode, P., Ostriker, J. P. & Turok, N. 2000, astro-ph/0010389
Boissier, S., Boselli, A., Prantzos, N. & Gavazzi, G. 2001, MNRAS, 321, 733
Bower, R. G., Lucey, J. R. & Ellis, R. S., 1992, MNRAS, 254, 589
Brinchmann, J. 1999, PhD thesis, Univ. Cambridge
Brinchmann, J. & Ellis, R. S. 2000, ApJ, 536, L77
Charlot, S., Worthey, G. & Bressan, A. 1996, ApJ, 457, 625
Cole, S., Lacey, C. G., Baugh, C. M. & Frenk, C. S. 2000, MNRAS, 319, 168
Colín, P., Avila-Reese, V. & Valenzuela, O. 2000, ApJ, 542, 622
Combes, F. 2000, astro-ph/0007318
Combes, F. 1999, astro-ph/9910296
de Grijs, R. & Peletier, R. F. 1999, MNRAS, 310, 157
Faber, S. M. & Jackson, R. 1976, ApJ, 204, 668
Ferguson, A. M. N., Wyse, R. .F. G., Gallagher, J. S. & Hunter, D. A. 1998, ApJ, 506, L19
Ferrara, A. & Tolstoy, E. 2000, MNRAS, 313, 291
Ferreras, I. & Silk, J. 2000a, ApJ, 532, 193
Ferreras, I. & Silk, J. 2000b, MNRAS, 316, 786
Giovanelli, R., Haynes, M. P., Herter, T., Vogt, N. P., Wegner, G., Salzer, J. J., Da Costa, L. N. & Freudling, W. 1997, AJ, 113, 22
Gnedin, N. Y. 1998, MNRAS, 294, 407
Ibata, R. A. & Gilmore, G. F. 1995, MNRAS, 275, 605
Jacoby, G. H. et al. 1992, PASP, 104, 599
Kauffmann, G., White, S. D. M. & Guiderdoni, G. 1993, MNRAS, 264, 201
Kauffmann, G., Colberg, J. M., Diaferio, A. & White, S. D. M. 1999, MNRAS, 303, 188
Kennicutt, R. C. 1983, ApJ, 272, 54
Kennicutt, R. C., Tamblyn, P. & Congdon, C. W. 1994, ApJ, 435, 22
Kennicutt, R. C. 1998a, ARA&A, 36, 189
Kennicutt, R. C. 1998b, ApJ, 498, 541
Kodama, T., Arimoto, N., Barger, A. J. & Aragón-Salamanca, A. 1998, A&A, 334, 99
Lacey, C. & Silk, J. 1991, ApJ, 381, 14
Larson, R. B. 1974, MNRAS, 169, 229
Lilly, S. J., Tresse, L., Hammer, F., Crampton, D. & Le Fèvre, O. 1995, ApJ, 455, 108
McGaugh, S. S., Schombert, J. M., Bothun, G. D. & de Blok, W. J. G. 2000, ApJ, 533, L99
MacLow, M.-M. & Ferrara, A. 1999, ApJ, 513, 142
Mathewson, D. S. & Ford, V. L. 1996, ApJS, 107, 97

Mo, H. J., Mao, S. & White, S. D. M. 1998, MNRAS, 295, 319
Olszewski, E. W., Suntzeff, N. B. & Mateo, M. 1996, ARA&A, 34, 511
Rich, R. M. 1990, ApJ, 362, 604
Rocha-Pinto, H. J. & Maciel, W. J. 1996, MNRAS, 279, 447
Salpeter, E. E. 1955, ApJ, 121, 161
Scalo, J. M. 1986, fund. Cosm. Phys., 11, 1
Schaller, G., Schaerer, D., Maeder, A. & Meynet, G. 1992, A&AS, 96, 269
Schmidt, M. 1959, ApJ, 129, 243
Silk, J. 1997, ApJ, 481, 703
Silk, J. 2000, MNRAS, in press, astro-ph/0010624
Simard, L. & Pritchet, C. J. 1998, ApJ, 505, 96
Somerville, R. S. & Primack, J. R. 1999, MNRAS, 310, 1087
Tinsley, B. M. 1980, Fund. Cosm. Phys., 5, 287
Tully, R. B. & Fisher, J. R. 1977, A&A, 54, 661
Tully, R. B., Verheijen, M. A. W., Pierce, M. J., Huang, J.-S. & Wainscoat, R. J. 1996, AJ, 112, 2471
Valentijn, E. A. & van der Werf, P. 1999, ApJ, 522, L29
Verheijen, M. A. W. 1997, PhD thesis, Univ. Groningen
Vogt, N. P., et al. 1997, ApJ, 479, L121
Vogt, N. P. 2000, in Combes, F., Mamon, G. A. & Charmandaris, V., eds, ASP Conf. Ser. 197, Dynamics of Galaxies: from the Early Universe to the Present. Astron. Soc. Pac., San Francisco, p. 435
White, S. D. M. & Rees, M. J. 1978, MNRAS, 183, 341
White, S. D. M. & Frenk C. S. 1991, ApJ, 379, 52
Worthey, G., Dorman, B. & Jones, L. A., 1996, AJ, 112, 948
Young, J. S. & Knezek, P. M. 1989, ApJ, 347, L55
Young, J. S., Allen, L., Kenney, J. D. P., Lesser, A. & Rownd, B. 1996, AJ, 112, 1903
Zaritsky, D., Kennicutt, R. C. & Huchra, J. P. 1994, 420, 87